Modulational stability and gap solitons of gapless systems: Continuous versus discrete limits

Matteo Conforti,[1,*] Costantino De Angelis,[1] T. R. Akylas,[2] and Alejandro B. Aceves[3]
[1]*CNISM, Dipartimento di Ingegneria dell'Informazione, Università degli Studi di Brescia, Brescia 25123, Italy*
[2]*Department of Mechanical Engineering, Massachusetts Institute of Technology, Cambridge, Massachusetts 02139, USA*
[3]*Department of Mathematics, Southern Methodist University, Dallas, Texas 75275, USA*
(Received 14 May 2012; published 26 June 2012)

We consider a model consisting of two subsystems with crossing linear dispersion curves that describes, for example, light propagation in binary waveguide arrays. This model admits bright-dark gap solitons in both the discrete and the continuous (long-wavelength) limits, in spite of the absence of a gap in the linear (i.e., plane-wave) spectrum. We find that these solitons are always modulationally unstable in the continuous limit, whereas they can be stable in the discrete system if the amplitude of the background component exceeds a certain threshold.

DOI: 10.1103/PhysRevA.85.063836 PACS number(s): 42.65.Tg, 78.67.Pt, 42.65.Sf

I. INTRODUCTION

Discrete optics in coupled waveguides has received intensive study during the last three decades [1]. Besides being an interesting research area on its own, due to several applications, for example in communication systems and optical computing, it furnishes a unique test bed for the observation of linear and nonlinear phenomena occurring in various branches of science due to the very general character of the underlying equations. This formal analogy has been exploited to mimic a variety of phenomena in the realm of (nonrelativistic) quantum mechanics [2], quantum field theory [3], and relativistic quantum mechanics [4,5], with particular emphasis on binary waveguide arrays [6,7]. Binary arrays with different coupling coefficients have been considered, since they might offer a feasible experimental framework in which to explore a two-band structure in the linear and nonlinear regimes [8,9]. In this scenario, the use of photonic crystal waveguides [10] or waveguides based on plasmonic confinement [11,12] offers a unique setting in which to exploit propagation in the so-called alternating positive and negative coupling regime [13,14]. In this instance, if the coupling coefficients have different moduli, a gap centered at zero Bloch momentum in the linear dispersion relation opens, allowing the existence of bright gap solitons [15,16]. However, if the coupling coefficients have equal moduli, the gap closes, and a "diabolical" or "Dirac" point emerges in the band structure at zero transverse momentum [13]. Despite the absence of a gap in the linear spectrum, which may prevent the existence of bright gap solitons [17], nonlinearity could in principle open a gap, allowing for the existence of gap solitons sitting on a nonvanishing constant background [18,19].

In this article we show that a nonlinearity-induced gap can appear in the plane-wave (PW) spectrum of a binary array with equal coupling coefficients if the nonlinear coefficients in the even and odd sites are different. We analyze the stability of the PW solutions in both the discrete case and in the continuous long-wavelength limit. It turns out that only the discrete system can support stable plane-wave propagation. Moreover, we find that highly localized discrete solitons can propagate in a stable fashion if the PW background amplitude exceeds a certain threshold. This perhaps surprising result, to the best of our knowledge, has not been observed in similar systems.

II. PHYSICAL SETTINGS

According to coupled mode theory (CMT) and taking into account third-order nonlinearities in the form of a pure Kerr effect, the governing equations read [15,20]:

$$i E'_{nz} + \beta_n E'_n + C_{n-1} E'_{n-1} + C_{n+1} E'_{n+1} + \chi_n |E'_n|^2 E'_n = 0,$$

where E'_n is the amplitude of the modal field $M_n(x)$ of the nth waveguide; β_n is the propagation constant of each individual waveguide ($\beta_n = \beta + \Delta\beta/2$ for n even and $\beta_n = \beta - \Delta\beta/2$ for n odd); χ_n, the site-dependent nonlinear coefficient, is γ_1 (γ_2) for n even (odd); and C_{n-1}, C_{n+1} are the coupling coefficients with the $(n-1)$th and the $(n+1)$th waveguide, respectively. In the specific case of interest, $C_{n-1} = C_1$ and $C_{n+1} = C_2$ when n is even, whereas $C_{n-1} = C_2$ and $C_{n+1} = C_1$ when n is odd. We then perform the transformation $E'_n = E_n \exp(i\beta z)$ and we separately consider the mode amplitudes in the even and odd waveguides. Finally, $E_{2n} = A_n$ and $E_{2n-1} = B_n$ are governed by the following two sets of coupled equations with constant coefficients:

$$\begin{aligned} i A_{nz} + \frac{\Delta\beta}{2} A_n + C_1 B_n + B_{n+1} + \gamma_1 |A_n|^2 A_n = 0, \\ i B_{nz} - \frac{\Delta\beta}{2} B_n + A_{n-1} + C_1 A_n + \gamma_2 |B_n|^2 B_n = 0, \end{aligned} \tag{1}$$

where without loss of generality C_2 has been set equal to 1.

Assuming Bloch-wave disturbances, $(A_n, B_n) \propto \exp\{i(nk_x + k_z z)\}$, the linear dispersion relation of Eqs. (1) reads

$$k_z^2 = \left(\frac{\Delta\beta}{2}\right)^2 + C_1^2 + 1 + 2C_1 \cos k_x.$$

Note that a band gap opens whenever $\Delta\beta \neq 0$ and/or for $C_1 \neq \pm 1$, the band edges corresponding to the wave number $k_x = 0$ for $C_1 < 0$ and $k_x = \pi$ for $C_1 > 0$. Moreover, it was demonstrated that discrete solitons can reside inside this gap [15,20].

*matteo.conforti@ing.unibs.it

 ©2012 American Physical Society

In what follows, we concentrate on the gapless system, which is obtained by posing $\Delta\beta = 0$ and $C_1 = -1$:

$$\begin{aligned} i A_{nz} + B_{n+1} - B_n + \gamma_1 |A_n|^2 A_n = 0, \\ i B_{nz} + A_{n-1} - A_n + \gamma_2 |B_n|^2 B_n = 0. \end{aligned} \tag{2}$$

In the neighborhood of $k_x = 0$, we use the expansions

$$A_{n\pm1}(z) = u(x,z) \pm u_x(x,z) + \tfrac{1}{2} u_{xx}(x,z) + \cdots,$$
$$B_{n\pm1}(z) = w(x,z) \pm w_x(x,z) + \tfrac{1}{2} w_{xx}(x,z) + \cdots,$$

to obtain (as a first-order approximation) the following continuous system in the long-wavelength limit:

$$\begin{aligned} i u_z + w_x + \gamma_1 |u|^2 u = 0, \\ i w_z - u_x + \gamma_2 |w|^2 w = 0. \end{aligned} \tag{3}$$

This system also arises in the neighborhood of $k_x = \pi$ for $C_1 = 1$, following a similar expansion procedure after the change of variables $(A_n, B_n) \to (-1)^n (A_n, B_n)$.

III. NONLINEAR DISPERSION AND MODULATIONAL STABILITY

A. Continuous limit

We start by looking for plane-wave solutions $u(x,z) = A \exp[i k_x x + i k_z z]$, $w(x,z) = B \exp[i k_x x + i k_z z]$ of the continuous system (3), for fixed total field intensity $I = |A|^2 + |B|^2$, to get

$$\begin{bmatrix} k_z - \gamma_1 |A|^2 & -i k_x \\ i k_x & k_z - \gamma_2 |B|^2 \end{bmatrix} \begin{bmatrix} A \\ B \end{bmatrix} = 0. \tag{4}$$

It turns out that the PW amplitude $|A|$ and wave number k_z must satisfy

$$k_x^2 = (k_z - \gamma_1 |A|^2)(k_z - \gamma_2 |B|^2), \tag{5}$$

$$|A|^2 = \frac{k_z - \gamma_2 |B|^2}{k_z - \gamma_1 |A|^2} |B|^2, \tag{6}$$

$$I = |A|^2 + |B|^2, \tag{7}$$

where Eq. (5) is derived from the determinant of the coefficient matrix of the vector $[A, B]^T$ and Eq. (6) is obtained by subtracting the first of Eqs. (4) multiplied by A^* from the conjugate of the second of Eqs. (4) multiplied by B.

After some algebra we can find $|A|^2$ as the roots of the fourth-order polynomial

$$\begin{aligned} &(\gamma_1 + \gamma_2)^2 |A|^8 - I(\gamma_1 + \gamma_2)(\gamma_1 + 3\gamma_2)|A|^6 \\ &\quad + \left[\gamma_2 I^2 (2\gamma_1 + 3\gamma_2) + 4k_x^2\right] |A|^4 \\ &\quad - I\left(\gamma_2^2 I^2 + 4k_x^2\right) |A|^2 + k_x^2 I^2 = 0, \end{aligned} \tag{8}$$

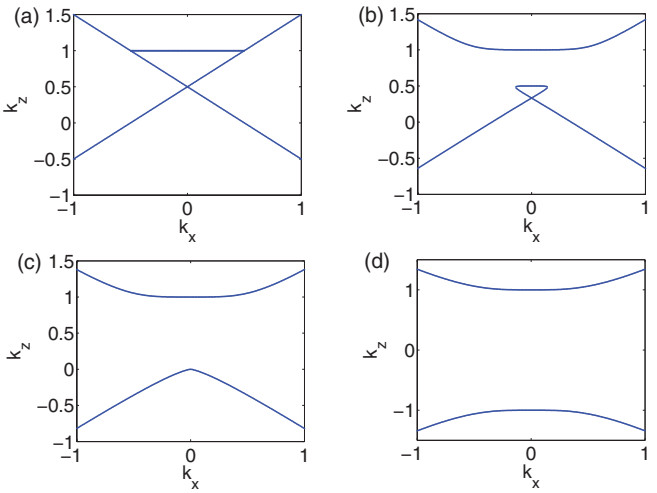

FIG. 1. (Color online) Dispersion relation for $I = 1$ and (a) $\gamma_1 = \gamma_2 = 1$; (b) $\gamma_1 = 1$, $\gamma_2 = 0.5$; (c) $\gamma_1 = 1$, $\gamma_2 = 0$; and (d) $\gamma_1 = 1$, $\gamma_2 = -1$.

and the wave number k_z from

$$k_z = \frac{\gamma_1 |A|^4 - \gamma_2 |B|^4}{|A|^2 - |B|^2}. \tag{9}$$

Examples of the computed dispersion relations are shown in Fig. 1. For a homogeneous array $\gamma_1 = \gamma_2$, the nonlinear dispersion relation does not show any gap. However, as soon as $\gamma_1 \neq \gamma_2$ a gap opens, and it widens upon increasing nonlinear nonhomogeneity.

We now perform a standard linear stability analysis (LSA) in order to analyze the modulational stability of the PW solutions. As usual we consider the ansatz $u(z,x) = [A + p_1(z,x)] \exp[i k_x x + i k_z z]$, $w(z,x) = [B + p_2(z,x)] \exp[i k_x x + i k_z z]$ that when inserted in Eqs. (3) gives the following linearized system for the small perturbations ($|p_1| \ll |A|$, $|p_2| \ll |B|$):

$$\begin{aligned} i p_{1z} + p_{2x} - k_z p_1 + i k_x p_2 + \gamma_1 (A^2 p_1^* + 2|A|^2 p_1) = 0, \\ i p_{2z} - p_{1x} - k_z p_2 - i k_x p_1 + \gamma_2 (B^2 p_2^* + 2|B|^2 p_2) = 0. \end{aligned} \tag{10}$$

By writing the perturbations as the sum of a Stokes–anti-Stokes pair as $p_m = \varepsilon_{s,m}(z) \exp[iqx] + \varepsilon_{a,m}(z) \exp[-iqx]$, we can write the first-order system for $\varepsilon = [\varepsilon_{1,s}, \varepsilon_{1,a}^*, \varepsilon_{2,s}, \varepsilon_{2,a}^*]^T$

$$\dot{\varepsilon} = M \varepsilon, \tag{11}$$

where

$$M = i \begin{bmatrix} 2\gamma_1 |A|^2 - k_z & \gamma_1 A^2 & i(k_x + q) & 0 \\ -\gamma_1 A^{2*} & -(2\gamma_1 |A|^2 - k_z) & 0 & i(k_x - q) \\ -i(k_x + q) & 0 & 2\gamma_2 |B|^2 - k_z & \gamma_2 B^2 \\ 0 & -i(k_x - q) & -\gamma_2 B^{2*} & -(2\gamma_2 |B|^2 - k_z) \end{bmatrix}.$$

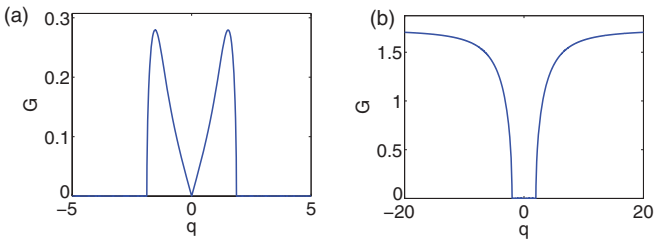

FIG. 2. (Color online) Modulational instability gain for $I = 4$, $k_x = 1$, $\gamma_1 = 1$, $\gamma_2 = 0.5$. (a) Lower branch and (b) upper branch of dispersion relation.

If for a fixed disturbance wave vector q the matrix M possesses at least one eigenvalue with nonvanishing real part, the PW solution will be unstable, and the perturbation will grow with a rate $G(q) = \max_{i=1,4}[\mathrm{Re}\{\lambda_i\}]$, λ_i being the eigenvalues of the matrix M.

We found that the plane-wave solutions are always modulationally unstable. In particular the PW solutions corresponding to the upper branch of the dispersion relation are unstable for high-disturbance wave number q, whereas the solutions corresponding to the lower branch show the usual instability gain profile, similar to the focusing nonlinear Schrödinger equation [21]. Figure 2 shows two representative examples.

B. Discrete problem

We now analyze the discrete system (2) in order to understand if the transition from a continuous system to a discrete one can change the LSA scenario. For the purpose of analyzing the crossover region, we write Eqs. (2) as the limit for $N \to \infty$ of the continuous systems:

$$\begin{aligned} iu_z + \sum_{n=1}^{N} \frac{w_{x^n}}{n!} + \gamma_1 |u|^2 u = 0, \\ iw_z + \sum_{n=1}^{N} \frac{(-1)^n u_{x^n}}{n!} + \gamma_2 |w|^2 w = 0. \end{aligned} \tag{12}$$

Again we calculate the plane-wave solutions $u(x,z) = A\exp[ik_x x + ik_z z]$, $w(x,z) = B\exp[ik_x x + ik_z z]$ with fixed field intensity $I = |A|^2 + |B|^2$. We obtain that the PW amplitude and wave number must satisfy the same constraints of the continuous systems (6) and (7), with Eq. (5) replaced by

$$|\Sigma_k|^2 = (k_z - \gamma_1 |A|^2)(k_z - \gamma_2 |B|^2), \tag{13}$$

where $\Sigma_k = \sum_{n=1}^{N} (ik_x)^n / n!$. For the fully discrete problem ($N \to \infty$) we get $\Sigma_k = \exp[ik_x] - 1$, as expected from direct analysis of system (2).

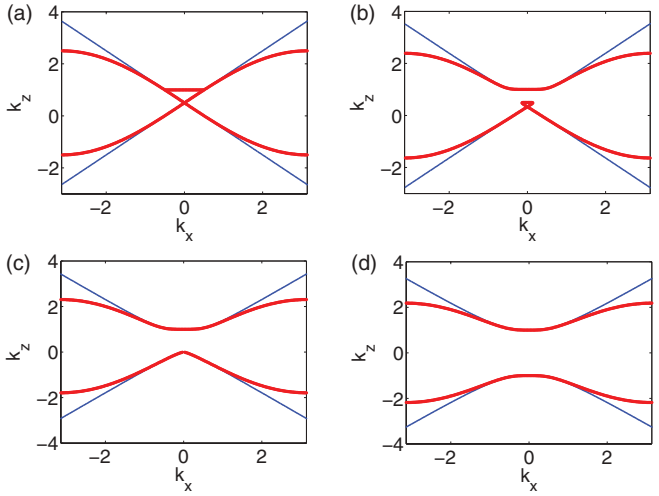

FIG. 3. (Color online) Dispersion relation for $I = 1$ and (a) $\gamma_1 = \gamma_2 = 1$; (b) $\gamma_1 = 1$, $\gamma_2 = 0.5$; (c) $\gamma_1 = 1$, $\gamma_2 = 0$; and (d) $\gamma_1 = 1$, $\gamma_2 = -1$. Thick (red) curve, discrete system; thin (blue) curve, long-wavelength limit.

After some algebra, we can find $|A|^2$ as the roots of the fourth-order polynomial,

$$\begin{aligned} &(\gamma_1 + \gamma_2)^2 |A|^8 - I(\gamma_1 + \gamma_2)(\gamma_1 + 3\gamma_2)|A|^6 \\ &\quad + [\gamma_2 I^2 (2\gamma_1 + 3\gamma_2) + 4|\Sigma_k|^2]|A|^4 \\ &\quad - I\left(\gamma_2^2 I^2 + 4|\Sigma_k|^2\right)|A|^2 + |\Sigma_k|^2 I^2 = 0, \end{aligned} \tag{14}$$

and the wave number k_z from Eq. (9).

Examples of the computed dispersion relations are shown in Fig. 3, superimposed with the corresponding ones for the long-wavelength limit.

We now perform LSA assuming as before $u(z,x) = [A + p_1(z,x)]\exp[ik_x x + ik_z z]$, $w(z,x) = [B + p_2(z,x)]\exp[ik_x x + ik_z z]$. Inserting this ansatz in Eqs. (12) gives the linearized system

$$\begin{aligned} &ip_{1z} + D_1 p_2 - k_z p_1 + \Sigma_k p_2 + \gamma_1 (A^2 p_1^* + 2|A|^2 p_1) = 0, \\ &ip_{2z} - D_2 p_1 - k_z p_2 + \Sigma_k^* p_1 + \gamma_2 (B^2 p_2^* + 2|B|^2 p_2) = 0, \end{aligned} \tag{15}$$

where D_1 and D_2 are the differential operators defined in Eqs. (12).

By writing the perturbations as before, $p_m = \varepsilon_{s,m}(z)\exp[iqx] + \varepsilon_{a,m}(z)\exp[-iqx]$, we can write the first-order system

$$\dot{\varepsilon} = Q\varepsilon, \tag{16}$$

where

$$Q = i \begin{bmatrix} 2\gamma_1|A|^2 - k_z & \gamma_1 A^2 & \Sigma_k + \Sigma_q & 0 \\ -\gamma_1 A^{2*} & -(2\gamma_1|A|^2 - k_z) & 0 & -\Sigma_k^* - \Sigma_q \\ \Sigma_k^* + \Sigma_q^* & 0 & 2\gamma_2|B|^2 - k_z & \gamma_2 B^2 \\ 0 & -\Sigma_k - \Sigma_q^* & -\gamma_2 B^{2*} & -(2\gamma_2|B|^2 - k_z) \end{bmatrix},$$

where $\Sigma_q = \sum_{n=1}^{N} (iq)^n / n!$.

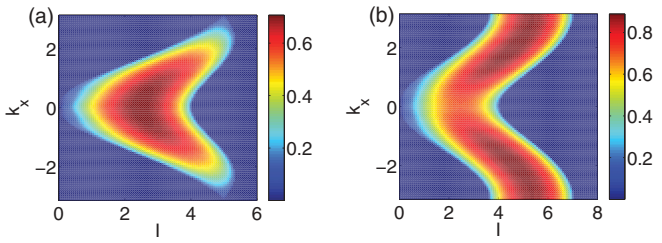

FIG. 4. (Color online) Modulational instability gain maps for (a) $\gamma_1 = 1$, $\gamma_2 = 0$ and (b) $\gamma_1 = 1$, $\gamma_2 = 0.5$.

Interestingly enough, we find that the plane-wave solutions for the discrete system can be modulationally stable. In particular we found that the PW solutions corresponding to the upper branch of the dispersion relation can be stable for high enough values of intensity I. Figure 4 shows maximum modulational instability gain as a function of intensity and wave number of the PW solutions for two representative examples. Observe that in both cases the (colored) region of instability is confined to a range of finite intensities.

Figure 5(a) shows the instability gain for an unstable PW of the discrete system, consisting in two bands centered around $q = \pm\pi$ (red curve). The modulational instability (MI) gain for the long-wavelength limit $N = 1$ consists of two bands with $|q| > q_0$ (blue curve); by increasing N the bands of the discrete system are well approximated, but the high-frequency bands do not disappear (black curves). Figure 5(b) shows that these high-frequency bands exist also when the discrete system does not manifest instability. The different behavior of discrete and continuous systems can be ascribed the periodicity. In fact the discrete system is periodic in the wave-number domain, and all the relevant features are contained in the first Brillouin zone $q \in [-\pi,\pi]$.

Some analytical calculations can be performed by taking $k_x = 0$. In this case $\Sigma_k = k_x = 0$, and the PW solutions of the discrete and continuous system coincide. We find from Eq. (14) that the PW solution sitting on the upper branch is given by $|A|^2 = I$, $B = 0$, and $k_z = \gamma_1 I$. Moreover, we can calculate the eigenvalues of the matrix Q/i:

$$\lambda = \pm\sqrt{|\Sigma_q|^2 + \tfrac{1}{2}\gamma_1^2 I^2 \pm \tfrac{1}{2}\gamma_1 I\sqrt{\gamma_1^2 I^2 - 4|\Sigma_q|^2}}. \quad (17)$$

The solution is stable if λ are real for all values of wave-number disturbance q, so the intensity must satisfy $\gamma_1^2 I^2 > 4|\Sigma_q|^2$. In the long-wavelength limit $|\Sigma_q|^2 = q^2$, so the solution is always unstable with respect to high enough wave-vector disturbance. However, in the discrete case $|\Sigma_q|^2 = 2 - 2\cos(q)$, entailing that PW solutions with $I > 4/|\gamma_1|$ are stable.

To conclude, the main result of this section is that PW solutions are always modulationally unstable in the continuous long-wavelength limit, whereas they can become stable in the discrete case for high enough intensity. This feature is quite counterintuitive, because in the standard modulational instability scenario, the higher is the intensity, the higher is the modulational instability gain [21].

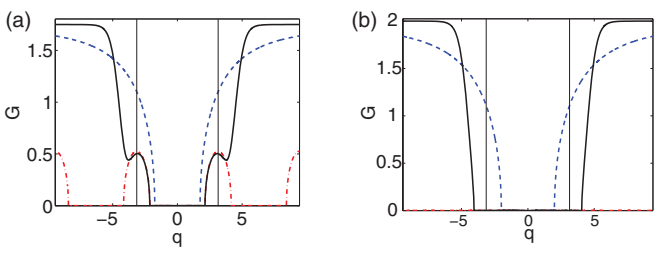

FIG. 5. (Color online) Modulational instability gain for $k_x = 0$, $\gamma_1 = 1$, $\gamma_2 = 0$: (a) $k_z = I = 3.5$, (b) $k_z = I = 4$. Dash-dotted (red) curves, discrete system; dashed (blue) curves, $N = 1$; solid black curves, $N = 8$. Vertical curves delimit the first Brillouin zone $[-\pi,\pi]$.

IV. DARK SOLITONS

A. Long-wavelength limit

We restrict ourselves to the simple interlaced linear-nonlinear case ($\gamma_1 \neq 0$, $\gamma_2 = 0$) and stationary solitons ($k_x = 0$) [22]. Despite its simplicity, this case contains all the relevant physics. More complex walking solitons of the general nonlinear case ($\gamma_1 \neq 0$, $\gamma_2 \neq 0$, $k_x = 0$), which can be found by Hamiltonian methods [15], are not considered here in order to keep the treatment as simple as possible. The simple bright-dark soliton reads

$$u(x,z) = \sqrt{\frac{\mu}{\gamma_1}}\tanh\left(\frac{\mu x}{\sqrt{2}}\right)e^{i\mu z},$$
$$w(x,z) = -\sqrt{\frac{\mu}{2\gamma_1}}\operatorname{sech}^2\left(\frac{\mu x}{\sqrt{2}}\right)e^{i\mu z}. \quad (18)$$

This solution sits on the PW characterized by intensity $I = \mu/\gamma_1$, wave number $k_z = \mu$, and amplitude $|A|^2 = I$, $|B| = 0$. From the previous section we know that this PW is always unstable in the continuous limit, entailing the instability of the soliton. This scenario is confirmed by numerical solution of Eqs. (3) with Eqs. (18) as the initial condition plus small noise (Fig. 6). The high-wave-number modulational instability corrupts the soliton profile after some propagation distance.

This solution, however, can in principle be stable in the discrete system. In fact we showed that an intensity threshold exists in the discrete system that permits PW solutions to be stable. With intensity $I > 4/|\gamma_1|$ solutions (18) sit on a stable background for the discrete system. However, the width of the solitons scales as $1/I$, entailing that the widest stable soliton has width $\approx\sqrt{2}/\mu \approx 0.35$. In this case, the long-wavelength limit breaks down, making the solutions a bad approximation for the discrete system. This case is well represented in Fig. 7, where solution (3) is used as the initial condition for system

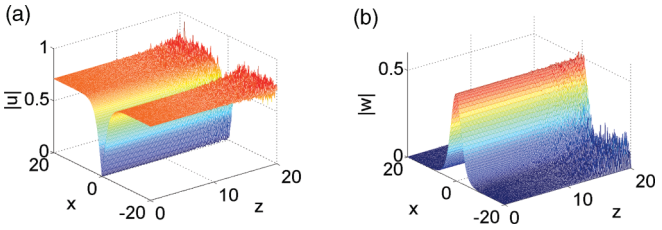

FIG. 6. (Color online) Propagation of a dark-bright soliton: $\gamma_1 = 1$, $\gamma_2 = 0$, and $I = 0.5$.

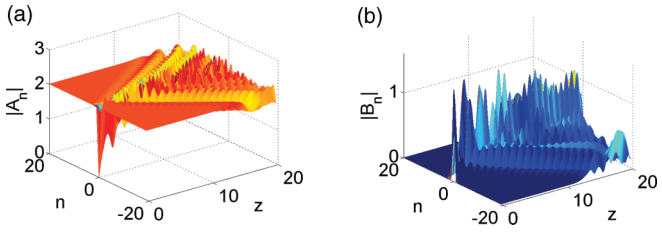

FIG. 7. (Color online) Failure of the continuous model for strongly localized beams. In the figure we report the numerical integration of Eqs. (2) using an initial condition corresponding to a very localized dark-bright soliton solution of the continuous system ($\gamma_1 = 1$, $\gamma_2 = 0$, $I = 4$).

(2). Due to the presence of high-wave-vector components, the initial profile is destroyed after a short propagation distance.

B. Strongly localized solitons

From the analysis above, we expect that discrete stable solitons will be strongly localized. Again we concentrate on the linear-nonlinear case $\gamma_2 = 0$ and $\gamma_1 \neq 0$, and without loss of generality we assume $\gamma_1 = \sigma = \pm 1$. In this case the PW solution is characterized by $k_z = \sigma I$, $|A|^2 = I$, $|B| = 0$. We try to find discrete solitons with the ansatz $A_n = a_n \exp[i\lambda\sigma z]$, $B_n = b_n \exp[i\lambda\sigma z]$, where $\lambda = I > 0$. We find from Eqs. (2)

$$b_n = \frac{1}{\sigma\lambda}(a_{n-1} - a_n), \tag{19}$$

$$(2 - \lambda^2)a_n - a_{n+1} - a_{n-1} + \lambda|a_n|^2 a_n = 0. \tag{20}$$

We write $a_n = \sqrt{\lambda}\hat{a}_n$ and assume $\hat{a}_n = O(1)$. Assuming a solution localized around the $n = 0$ waveguide, we consider a three-site solution [23]:

$$\begin{aligned} n = -1 &: (2 - \lambda^2)\hat{a}_{-1} - \hat{a}_0 - \hat{a}_{-2} + \lambda^2\hat{a}_{-1}^2\,\hat{a}_{-1}^* = 0, \\ n = 0 &: (2 - \lambda^2)\hat{a}_0 - \hat{a}_1 - \hat{a}_{-1} + \lambda^2\hat{a}_0^2\hat{a}_0^* = 0, \\ n = 1 &: (2 - \lambda^2)\hat{a}_1 - \hat{a}_2 - \hat{a}_0 + \lambda^2\hat{a}_1^2\hat{a}_1^* = 0. \end{aligned} \tag{21}$$

Assuming $\lambda \gg 1$ we make the following asymptotic expansion:

$$\begin{aligned} \hat{a}_{-2} &= -1 + \cdots, \\ \hat{a}_{-1} &= -1 + \frac{c_{-1}}{\lambda^2} + \cdots, \\ \hat{a}_0 &= \frac{c_0}{\lambda^2} + \cdots, \\ \hat{a}_1 &= s + \frac{c_1}{\lambda^2} + \cdots, \\ \hat{a}_2 &= -s + \cdots, \end{aligned}$$

where $s = \pm 1$ and $\hat{a}_{n<-2} = \hat{a}_{-2}$, $\hat{a}_{n>2} = \hat{a}_2$. Inserting the asymptotic expansion into Eqs. (21) we find the consistency relation for the coefficients c_n:

$$\begin{aligned} c_{-1} + c_{-1}^* &= 1, \\ c_0 &= 1 - s, \\ c_1 + c_1^* &= -s. \end{aligned}$$

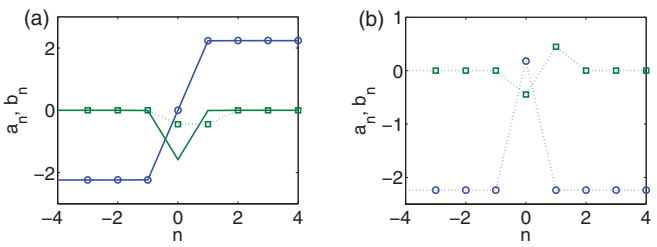

FIG. 8. (Color online) Strongly localized discrete solitons profile: $\lambda = 5$ and (a) $s = 1$, (b) $s = -1$. Circles, a_n; squares, b_n. Solid curves in (a) show the continuous soliton (18) sampled in the waveguide's positions.

For $s = 1$ we obtain the following solution (at the leading order in λ):

$$\ldots, a_{-1} = -\sqrt{\lambda}, \quad a_0 = 0, \quad a_1 = \sqrt{\lambda}, \ldots, \tag{22}$$

$$\ldots, b_{-1} = 0, \quad b_0 = -\frac{1}{\sigma\sqrt{\lambda}}, \quad b_1 = -\frac{1}{\sigma\sqrt{\lambda}}, \ldots, \tag{23}$$

whereas for $s = -1$ we get

$$\ldots, a_{-1} = -\sqrt{\lambda}, \quad a_0 = \frac{2}{\lambda^{3/2}}, \quad a_1 = -\sqrt{\lambda}, \ldots, \tag{24}$$

$$\ldots, b_{-1} = 0, \quad b_0 = -\frac{1}{\sigma\sqrt{\lambda}}, \quad b_1 = \frac{1}{\sigma\sqrt{\lambda}}, \ldots. \tag{25}$$

Two representative examples are shown in Fig. 8. For $s = 1$ we can also make a comparison with the sech-tanh soliton of the continuous system. While the dark component is well approximated by a hyperbolic tangent, the bright component is very different from the hyperbolic secant. The cause of the discrepancy is the fact that while the sech is peaked around $n = 0$, the discrete soliton has two equally high sites in $n = 0$ and $n = 1$, whereas the $s = -1$ soliton has no counterpart in the continuous system.

From the result of LSA we expect that discrete solitons will be unstable for $\lambda < 4$. In fact the numerical simulation reported in Fig. 9 for $\lambda = 3.5$, shows a destruction of the soliton profile after a short propagation distance. However, for $\lambda > 4$ we expect a stable propagation for the PW background; moreover,

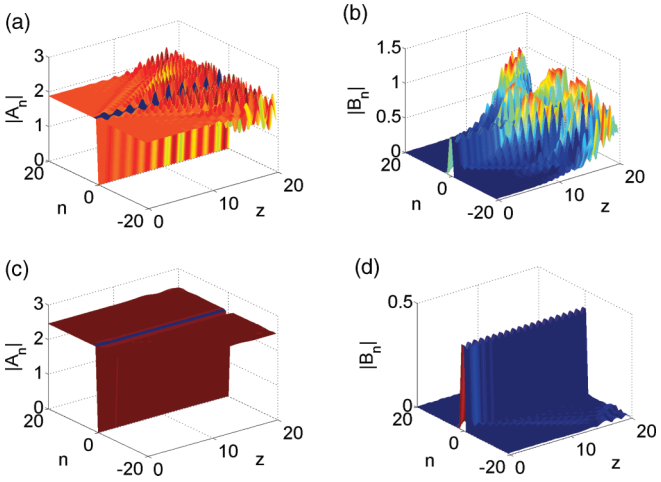

FIG. 9. (Color online) Propagation of discrete solitons for $s = 1$: (a, b) $\lambda = 3.5$, (c, d) $\lambda = 6$. Similar behavior is obtained for $s = -1$.

λ being sufficiently high, we expect that the asymptotic expansion at first order will give a good estimate for the soliton profile. This is indeed the case, as shown in Fig. 9, where a stable propagation is evident, together with a very low emission of radiation, for $\lambda = 6$.

V. CONCLUSIONS

We considered a model consisting of two equations coupled exclusively by nonlinear terms that describes light propagation in nonlinearly nonuniform binary waveguide arrays. We showed the existence of bright-dark gap solitons of both the discrete system and its continuous long-wavelength limit, in spite of the absence of a gap in the linear (i.e., plane-wave) spectrum. We find that these solitons are always modulationally unstable in the continuous limit, whereas they can be stable in the discrete system if the amplitude of the dark component exceeds a certain threshold.

ACKNOWLEDGMENTS

Work was done in part under the UniBSMIT-MechE faculty exchange program co-sponsored by the CARIPLO Foundation, Italy, under Grant No. 2008-2290. C.D.A. and M.C. acknowledge financial support from the CARIPLO Foundation under Grant No. 2010-0595 and from the U.S. Army under Grant No. W911NF-11-1-0285. A.A. would like to thank the University of Brescia collaborators for their hospitality during his recent visit. A.A. acknowledges support from the U.S. National Science Foundation under Grant No. ECCS-1128593.

[1] F. Lederer, G. I. Stegeman, D. N. Christodoulides, G. Assanto, M. Segev, and Y. Silberberg, Phys. Rep. **463**, 1 (2008).
[2] S. Longhi, Laser Phot. Rev. **3**, 243 (2009).
[3] S. Longhi and G. Della Valle, Phys. Rev. A **85**, 012112 (2012).
[4] F. Dreisow, M. Heinrich, R. Keil, A. Tunnermann, S. Nolte, S. Longhi, and A. Szameit, Phys. Rev. Lett. **105**, 143902 (2010).
[5] O. Bahat-Treidel, O. Peleg, M. Grobman, N. Shapira, M. Segev, and T. Pereg-Barnea, Phys. Rev. Lett. **104**, 063901 (2010).
[6] S. Longhi, Phys. Rev. B **81**, 075102 (2010).
[7] S. Longhi, Phys. Rev. B **81**, 075102 (2010).
[8] M. Guasoni, A. Locatelli, and C. De Angelis, J. Opt. Soc. Am. B **25**, 1515 (2008).
[9] M. Guasoni, M. Conforti, and C. De Angelis, Opt. Commun. **283**, 1161 (2010).
[10] C. M. de Sterke, L. C. Botten, A. A. Asatryan, T. P. White, and R. C. McPhedran, Opt. Lett. **29**, 1384 (2004).
[11] M. Conforti, M. Guasoni, and C. De Angelis, Opt. Lett. **33**, 2662 (2008).
[12] S. H. Nam, E. Ulin-Avila, G. Bartal, and X. Zhang, Opt. Lett. **35**, 1847 (2010).
[13] S. H. Nam, A. J. Taylor, and A. Efimov, Opt. Express **18**, 10120 (2010).
[14] N. K. Efremidis, P. Zhang, Z. Chen, D. N. Christodoulides, C. E. Rüter, and Detlef Kip, Phys. Rev. A **81**, 053817 (2010).
[15] M. Conforti, C. De Angelis, and T. R. Akylas, Phys. Rev. A **83**, 043822 (2011).
[16] A. Marini, A. V. Gorbach, and D. V. Skryabin, Opt. Lett. **35**, 3532 (2010).
[17] R. Grimshaw and B. A. Malomed, Phys. Lett. A **198**, 205 (1995).
[18] Y. S. Kivshar, Phys. Rev. Lett. **70**, 3055 (1993).
[19] N. Flytzanis and B. A. Malomed, Phys. Lett. A **227**, 335 (1997).
[20] A. A. Sukhorukov and Y. S. Kivshar, Opt. Lett. **27**, 2112 (2002).
[21] G. P. Agrawal, *Nonlinear Fiber Optics*, 3rd ed. (Academic Press, San Diego, CA, 2001).
[22] K. Hizanidis, Y. Kominis, and N. K. Efremidis, Opt. Express **22**, 18296 (2008).
[23] A. B. Aceves, C. De Angelis, T. Peschel, R. Muschall, F. Lederer, S. Trillo, and S. Wabnitz, Phys. Rev. E **53**, 1172 (1996).